PRAMANA
— journal of
physics

Vol. 65, No. 5
November 2005
pp. 893–900

Magnetic properties of nanostructured spinel ferrites and nanocomposite $Nd_2Fe_{14}B/\alpha$-Fe permanent magnets

A NARAYANASAMY
Materials Science Centre, Department of Nuclear Physics, University of Madras, Guindy Campus, Chennai 600 025, India
E-mail: ansuom@yahoo.co.in

Abstract. This paper presents some of the important magnetic properties of the nanostructured spinel ferrites such as $Ni_{0.5}Zn_{0.5}Fe_2O_4$ and $Mn_{0.67}Zn_{0.33}Fe_2O_4$ and also that of the nanocomposite $Nd_2Fe_{14}B/\alpha$-Fe permanent magnetic material. The increase in the magnetic transition temperature of Ni–Zn ferrite from 538 K in the bulk state to 592 K when the grain size is reduced to 16 nm is correlated to the enhancement in the AB superexchange interaction strength because of an increase in the magnetic ion concentration in the A-site on milling, as shown by the EXAFS and in-field Mössbauer studies. The particle size has been tailor-made by varying the concentration of the oxidant in the case of Mn–Zn ferrite. The critical particle size for the superparamagnetic limit has been found to be 25 nm with an effective magnetic anisotropy constant of 7.78 kJ m^{-3} which is about an order of magnitude higher than that of the bulk ferrite. The exchange coupling is found to be strengthened in the nanocomposite magnet $Nd_2Fe_{14}B/\alpha$-Fe, when the grain boundary anisotropy is removed by thermal annealing and thus facilitating the enhancement of the energy product.

Keywords. Ferrites; superexchange interactions; magnetic properties of nanostructures; Mössbauer spectroscopy of solids.

PACS Nos 75.50.Gg; 75.75.+a; 76.80.+y; 75.30.Et

1. Introduction

Nanocrystalline magnetic materials find many applications in high-density magnetic recording media, magnetic hyperthermia, drug delivery systems etc. [1]. In this paper we report the details of the synthesis and magnetic properties of the $Ni_{0.5}Zn_{0.5}Fe_2O_4$ and $Mn_{0.67}Zn_{0.33}Fe_2O_4$ spinel ferrites and the nanocomposite permanent magnetic material $Nd_2Fe_{14}B/\alpha$-Fe. The latter material is important in the fabrication of high-energy density permanent magnets [2].

2. Experimental

The spinel ferrites $Ni_{0.5}Zn_{0.5}Fe_2O_4$ and $Mn_{0.67}Zn_{0.33}Fe_2O_4$ were synthesized using conventional solid-state reaction technique and oxidation method respectively. In

the case of Ni–Zn ferrite, metallic oxide powders were thoroughly mixed in the stoichiometric ratio and calcined at 1173 K in air for 5 h. The calcined powder was ground in an agate mortar, pelletized and sintered in air at 1473 K for 5 h. To produce various grain sizes, in order to study the grain size-dependence of the Néel temperature of the nanostructured Ni–Zn ferrite, the sample was milled in air using a planetary ball mill (Fritsch Pulverisette P7). Tungsten carbide vials and balls were used for milling and the ball-to-powder weight ratio was 8 : 1. The single phase spinel formation without any impurity was found from X-ray diffraction using Cu-K_α target. The EXAFS spectra at Ni and Zn K-edges were recorded at 300 K to study the structural changes on milling. The thermomagnetization curves were recorded using a thermogravimetric analyzer (TGA, Perkin-Elmer Series 7) with a small horse-shoe magnet (4 mT). The zero-field and in-field (6 T) Mössbauer spectra were recorded using a constant acceleration Mössbauer spectrometer with a ^{57}Co source diffused into a Rh matrix. In the case of $Mn_{0.67}Zn_{0.33}Fe_2O_4$, the reagents $FeSO_4{\cdot}7H_2O$, $MnCl_2{\cdot}4H_2O$, $ZnSO_4{\cdot}H_2O$ and $Fe_2(SO_4)_3$ were used keeping the Mn-to-Zn ratio as 2. NaOH was used for the metal hydroxide precipitation and KNO_3 was used to oxidize the ferrous ions to the ferric state. The final precipitate of the ferrite was washed several times using water and dried in an oven at 333 K for 48 h. The average particle size of the Mn–Zn ferrite was determined using a transmission electron microscope (TEM). Mössbauer spectra were recorded at 300, 200 and 16 K using a CTI make closed cycle helium cryostat. Magnetization studies were performed using a vibrating sample magnetometer at various temperatures in a maximum field of 1.2 T. An ingot of the nanocomposite $Nd_{10}Fe_{85}B_5$ permanent magnetic material was prepared by induction melting. By using a copper wheel, rotating with the speed of 40 m/s, the ingot was melt-spun in argon atmosphere and the melt-spun ribbon was annealed at 893 K for 20 min in vacuum.

3. Results and discussion

3.1 *$Ni_{0.5}Zn_{0.5}Fe_2O_4$ ferrite*

The average grain size for the Ni–Zn ferrite was calculated from the full-width at half-maximum of the (3 1 1) peak in the XRD pattern using the Scherrer's formula and is shown in figure 1 as a function of milling time. The lattice parameter is found to increase with milling, may be due to the change in cation distribution and bond stretching due to milling [3–5]. Figure 2 shows the thermogravimetric plots of Ni–Zn ferrite with a small applied field of 4 mT for two different grain sizes. The Néel temperature is found to increase for the milled samples, as shown in figure 1. The Néel temperature is 560 K for the unmilled sample, 592 K for the sample milled for 15 h whereas it is only 538 K for the bulk nickel zinc ferrite [6]. In order to investigate the changes in the cation distribution due to milling, which could be the cause for the increase in the Néel temperature, ^{57}Fe Mössbauer spectrum was recorded in an applied magnetic field of 6 T at 10 K (figure 3) and also the EXAFS study (figure 4) was carried out for the unmilled sample with 49 nm grain size and also for the 15 h milled sample with 16 nm grain size. The Mössbauer studies gave a value of 0.47 for the ratio of the population of the Fe^{3+} ions in A- and B-sites,

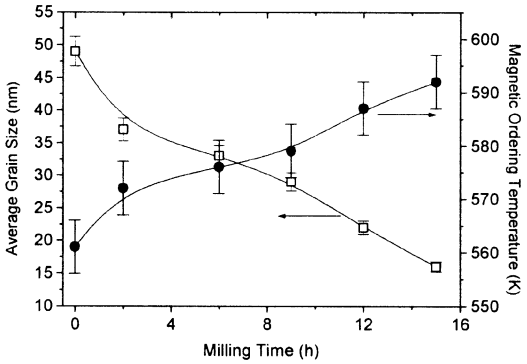

Figure 1. The variation of the average grain size and the magnetic ordering temperature of nanostructured $Ni_{0.5}Zn_{0.5}Fe_2O_4$ as a function of milling time.

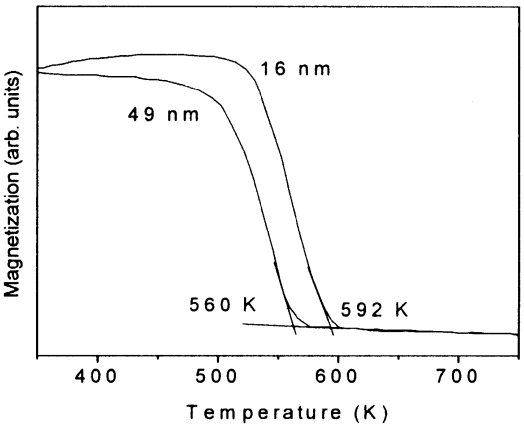

Figure 2. The thermogravimetric plot for the nanostructured $Ni_{0.5}Zn_{0.5}Fe_2O_4$ with average grain sizes 49 nm and 16 nm.

which is higher than the normally obtained value of 0.33 if all the Zn^{2+} ions are assumed to be on the A site and all the Ni^{2+} ions are on the B-site. Moreover, the EXAFS studies do not show any Zn^{2+} ions on the B-site for the unmilled sample. Therefore, the cation distribution for the unmilled sample can be written as $(Zn_{0.5}Fe_{0.64})[Ni_{0.5}Fe_{1.36}]O_4$ and it is interesting to note an unusual occupation of more than eight out of the sixty four of the A-sites in a unit cell. From the Fourier transform of the EXAFS spectrum at the Zn K-edge, we find an increase in the Zn^{2+}–O^{2-} distance in the milled sample in comparison to the unmilled one. This confirms a partial displacement of Zn^{2+} ions from A-site to B-site on milling. Even though the EXAFS at Ni K-edge does not show a visible change in the Ni^{2+}–O^{2-} distance to support unambiguously the displacement of Ni^{2+} ions from the B- to A-site on milling, one could not rule out such a possibility as one could infer from the EXAFS spectrum that the environment around Ni is different for the unmilled and milled samples. Thus an increase in the population of magnetic ions (Fe^{3+} and/or

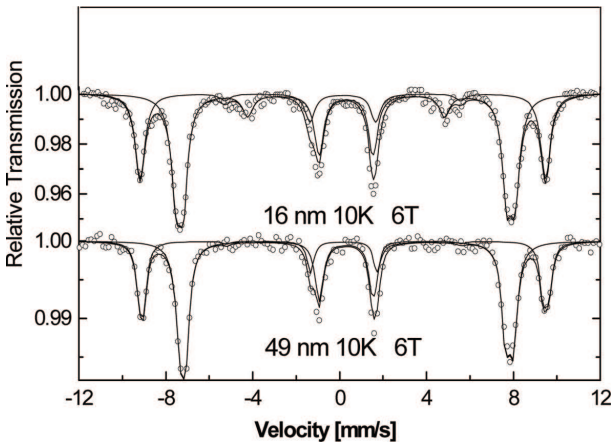

Figure 3. The Mössbauer spectra in an external magnetic field of 6 T applied parallel to the γ-ray direction for the unmilled and 15 h milled $Ni_{0.5}Zn_{0.5}Fe_2O_4$ samples.

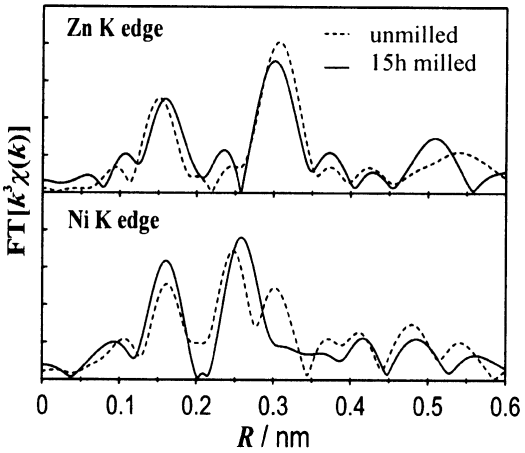

Figure 4. The Fourier-transform of the EXAFS spectrum of the unmilled and the 15 h milled $Ni_{0.5}Zn_{0.5}Fe_2O_4$ samples for Zn and Ni K edges.

Ni^{2+}) in the A-sites has strengthened the superexchange interaction between the two sites to account for the increase in the Néel temperature.

3.2 *$Mn_{0.67}Zn_{0.33}Fe_2O_4$ ferrite*

By varying the concentration of the oxidant (KNO_3) or ferric ions, we could achieve particle sizes ranging from 20 to 80 nm in the case of $Mn_{0.67}Zn_{0.33}Fe_2O_4$. The particle morphology was studied with TEM and one such TEM picture is shown in figure 5 for the 25 nm particles. The magnetization decreases with the decrease in

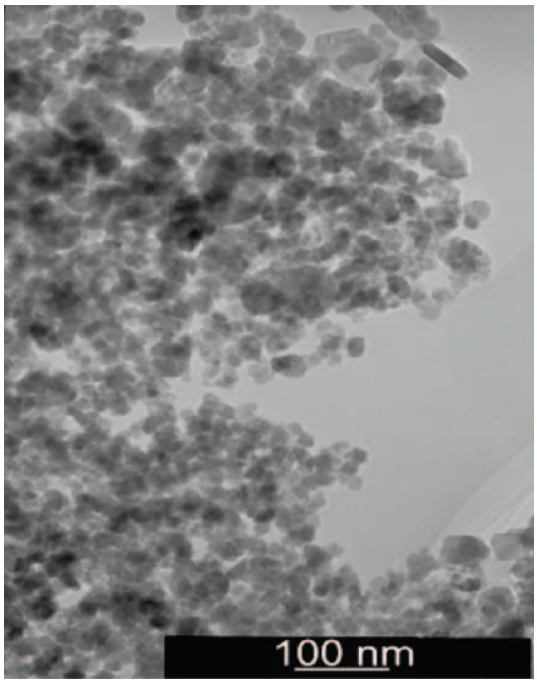

Figure 5. The TEM picture of the 25 nm particles of $Mn_{0.67}Zn_{0.33}Fe_2O_4$ sample.

the particle size and it is 49 A m^2 kg^{-1} for the 80 nm particles and 34 A m^2 kg^{-1} for the 20 nm particles. The blocking temperature T_B is given by

$$\tau = \tau_0 \exp(K_{\text{eff}} V / kT_B), \tag{1}$$

where K_{eff} is the effective magnetic anisotropy constant, V is the volume of the particle, k is the Boltzmann constant, τ is the relaxation time and τ_0 is the relaxation time constant. The time window of the Mössbauer experiment is 10^{-8} s. If the relaxation time τ is less than 10^{-8}, then the thermal energy makes the moments to fluctuate rapidly resulting in a doublet. At the blocking temperature T_B, the relaxation time τ is larger than the Mössbauer time window and hence a sextet is obtained in the Mössbauer spectrum. Since there is always a distribution in the relaxation time due to particle size distribution, the blocking temperature is taken as that temperature at which the doublet and sextet intensities are equal. In figure 6 we find that the doublet and sextet have almost equal intensities (48 : 52) at 293 K for the 25 nm particles and therefore T_B from the Mössbauer measurements turns out to be 293 K. Similarly T_B from the ZFC and FC magnetic measurements shown in figure 7 is found to be 135 K. With these data and using eq. (1) the effective magnetic anisotropy constant is calculated to be 7.78 kJ m^{-3}, which is an order of magnitude higher than that for the bulk Mn–Zn ferrite (1 kJ m^{-3}) of similar composition [7]. This enhancement is attributed to the surface anisotropy of the small particles.

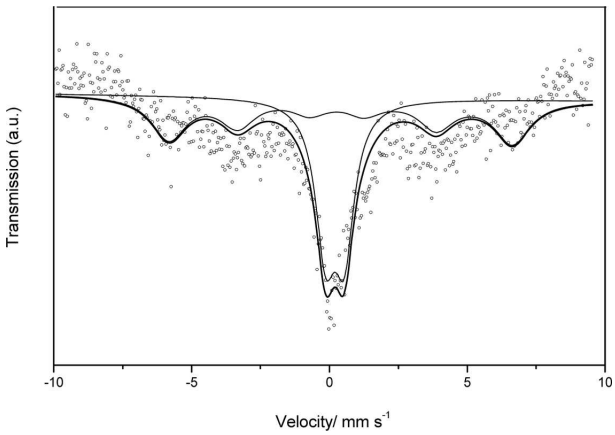

Figure 6. The Mössbauer spectrum at 300 K of the 25 nm particles of $Mn_{0.67}Zn_{0.33}Fe_2O_4$.

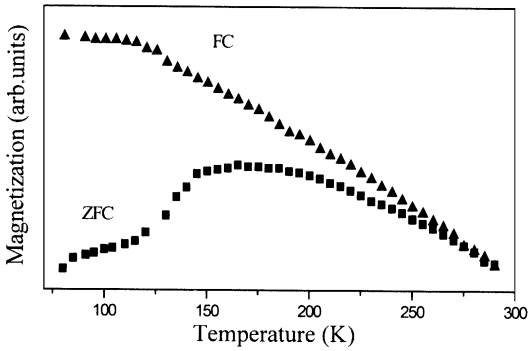

Figure 7. The zero-field cooled and field-cooled magnetization for the 25 nm particles of $Mn_{0.67}Zn_{0.33}Fe_2O_4$.

3.3 *$Nd_2Fe_{14}B/\alpha$-Fe nanocomposite*

The nanocomposite $Nd_2Fe_{14}B/\alpha$-Fe ribbons are crystalline containing $Nd_2Fe_{14}B$ and α-Fe phases. The average grain size for both the as-spun and annealed ribbons is around 36 nm for the $Nd_2Fe_{14}B$ grains and it is about 30 nm for the α-Fe grains. The ribbons exhibited enhanced remanence ratio compared to that of the Stoner–Wohlfarth particles, which may be due to exchange or dipolar coupling. Room temperature and high temperature δM measurements were, therefore, done to verify the nature of coupling. δM values are calculated from the isothermal remanence magnetization (IRM) measurement, which is done by plotting the remanent magnetization as a function of field from a demagnetized sample and from direct current demagnetization (DCD) measurements by applying a reverse field and measuring the demagnetization curve of the sample.

$$\delta M = \{M_D(H) - [M_r(H_{\max}) - 2M_R(H)]\}/M_r(H_{\max}) \tag{2}$$

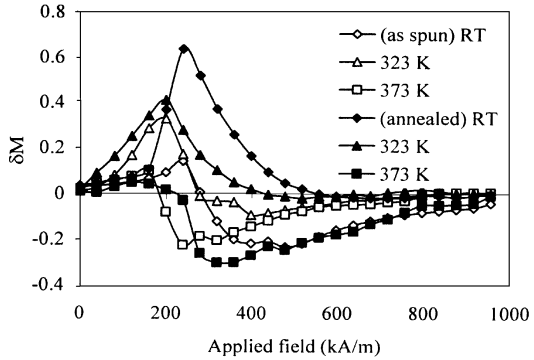

Figure 8. The δM plot of the as-spun and annealed $Nd_{10}Fe_{85}B_5$ ribbons at 293 K, 323 K and 373 K (open symbols represent the as-spun ribbons and the filled ones represent annealed ribbons).

is plotted as a function of applied field in figure 8. In this relation $M_D(H)$ is the DCD remanence, $M_R(H)$ is the IRM and $M_r(H_{\max})$ is the saturation remanence. A positive value for δM represents exchange interaction and the negative value represents dipolar interaction respectively between the crystals. The presence of both exchange and dipolar couplings for the as-spun ribbons at room temperature, an increase in the exchange coupling at 323 K and the presence of only the dipolar coupling at 373 K are very much obvious from figure 8. The existence of both the couplings is due to the presence of grain boundary anisotropy. On annealing, the grain boundary anisotropy is lowered resulting in an increase in the domain wall width according to the relation

$$\delta_{\mathrm{W}} = \pi\sqrt{(A/K)}, \tag{3}$$

where A is the exchange stiffness and K is the anisotropy constant. Because of the increase in the domain wall width, the exchange interaction extends over a larger distance. However, the increase in exchange coupling at 323 K is not observed in the annealed ribbons as the anisotropy has already been removed on annealing. At 373 K, the rapid decrease in magnetization with temperature reduces the exchange length and hence only dipolar coupling is observed and the Henkel plots published elsewhere [8] also support this conclusion. Our studies clearly show that the exchange interaction strength can be enhanced and thus higher energy products can be achieved by reducing the grain boundary anisotropy on thermal annealing.

4. Conclusion

In the case of Ni–Zn ferrite, the Néel temperature (T_{N}) is found to increase with grain size reduction. The replacement of the non-magnetic Zn^{2+} ions by the magnetic ions (Fe^{3+} and/or Ni^{2+}) at A-sites strengthens the A–B superexchange interaction and leads to an increase in the Néel temperature. In Mn–Zn ferrite, the critical particle size limit for superparamagnetism is found to be 25 nm at 300 K.

The higher value of the effective magnetic anisotropy constant 7.78 kJ m^{-3} for the 25 nm particle is attributed to the surface spin anisotropy of the small particles. In the $Nd_2Fe_{14}B/\alpha$-Fe nanocomposite, the exchange interaction between the grain is strengthened by removing the grain boundary anisotropy with thermal annealing.

Acknowledgment

We are grateful to J M Greneche for the in-field Mössbauer measurements, K Shinoda for the EXAFS measurements, B Jeyadevan for fruitful discussions and C N Chinnasamy, N Ponpandian, R Justin Joseyphus, N Sivakumar for various other measurements. The financial support from the DST, Govt. of India (Project No. SR/S5/NM-23/2002) is acknowledged.

References

[1] Q A Pankhrust, J Connolly, S K Jones and J Dobson, *J. Phys.* **D36**, R167 (2003)
[2] E F Kneller and R Hawig, *IEEE Trans. Magn.* **MAG-27**, 3588 (1991)
[3] L Wang and F S Li, *J. Magn. Magn. Mater.* **223**, 233 (2001)
[4] T Sato, T Iijima, M Seki and N Inagaki, *J. Magn. Magn. Mater.* **65**, 252 (1987)
[5] K Haneda and A H Morrish, *J. Appl. Phys.* **63,** 4258 (1988)
[6] J Smit and H P J Wijin, in *Ferrites* (Philips Technical Library, Eindhovan, The Netherlands, 1959) p. 157
[7] S Chikazumi, *Physics of magnetism* (John Wiley and Sons, New York, 1964) p. 141
[8] R Justin Joseyphus, A Narayanasamy, D Prabhu, L K Varga, B Jeyadevan, C N Chinnasamy, K Tohji and N Ponpandian, *Phys. Status Solidi.* **C1**, 3489 (2004)